

Finite Larmor Radius Effect on Ion-Temperature-Gradient Instability in Cylindrical Plasmas

Naohiro KASUYA^{1,2)}, Tomotsugu OHNO²⁾, Makoto SASAKI^{1,2)} and Masatoshi YAGI³⁾

¹⁾Research Institute for Applied Mechanics, Kyushu University, 6-1 Kasuga-Koen, Kasuga, Fukuoka 816-8580, Japan

²⁾Interdisciplinary Graduate School of Engineering Sciences, Kyushu University, 6-1 Kasuga-Koen, Kasuga, Fukuoka 816-8580, Japan

³⁾National Institutes for Quantum and Radiological Science and Technology, 2-166 Omotedate, Obuchi, Rokkasho-mura, Aomori 039-3212, Japan

(Received 6 June 2019 / Accepted 19 August 2019)

Numerical analyses using a gyro-fluid model have been performed to investigate the finite-Larmor-radius (FLR) effect on ion-temperature-gradient (ITG) instability in cylindrical plasmas. A spectrum code with Fourier-Bessel expansion has been developed for the analysis of global mode structures. The analytical expression of the η (ratio between the density and temperature gradient lengths) threshold value for linear ITG instability has been obtained from the local dispersion relation, whose dependency on the ion temperature comes from the FLR effect. Dependency of the threshold by the global analysis is reproduced by the local analysis with appropriate selection of the perpendicular wavenumber. Break of the Boltzmann relation by the FLR effect is not strong as to generate another unstable branch of the ITG mode.

© 2019 The Japan Society of Plasma Science and Nuclear Fusion Research

Keywords: gyro-fluid model, finite-Larmor-radius effect, linear device, ion-temperature-gradient instability, dispersion relation

DOI: 10.1585/pfr.14.1401158

1. Introduction

Numerical simulations of micro-scale turbulence have been carried out to identify the cause for transport in magnetic confined fusion plasmas. Several gyro-kinetic simulation codes have been developed for that purpose, and local linear stability analyses for several kinds of modes, formation mechanism of global turbulent structures and their dynamics can be studied [1]. On the other hand, gyro-fluid models have been also used for transport analysis. Computational costs are reduced compared with gyro-kinetic simulations, so are advantage in carrying out parameter scans and global simulations of turbulence. Transport models GLF23 and TGLF are developed based on the gyro-fluid model [2–4]. Three-dimensional turbulence simulations are carried out for toroidal ion-temperature-gradient (ITG) turbulence [5], and dynamical phenomena, as ELM burst, are also studied [6]. Spatio-temporal causal relations included in a wide range of plasma regions is one of the keys for transport mechanism, so a simulation scheme efficient for global analysis is needed.

Clarifying fundamental mechanisms of turbulence is important [7], and researches on structural formation of plasma turbulence have been progressing by using linear devices [8]. A linear device has a cylindrical shape without magnetic curvature and can produce high density plasmas, so is suitable for basic experiments to observe plasma instabilities in details [9, 10]. Numerical simulations of lin-

ear devices have been also carried out, and a reduced fluid model for drift wave turbulence is used to describe the 3-D turbulence [11]. For understanding structural formation mechanism, identification of the spatial structure of eigenmodes is important as drive of turbulence. In basic experimental devices, the typical spatial scales of the device and gyro-motion of ions are close to each other, so the finite Larmor radius (FLR) effect is not negligible. A mode with the wave length comparable to the effective ion Larmor radius can become unstable even in low ion temperature plasmas [12]. For the first step, linear characteristic of the ITG instability has been investigated using the parameter set of PANTA linear device [13]. Here we have developed a global simulation code for the ITG instability in linear devices [14]. The parameter dependency is evaluated with a gyro-fluid model to identify influence of the FLR effect, and is compared with analytical expression obtained from a linear dispersion relation in this article.

2. Model

Fluid models are used for analyzing global mode structures in collisional plasmas. The following set of linearized gyro-fluid equations [15] is used, where the magnetic curvature terms can be eliminated for the analysis of the cylindrical configuration;

$$\frac{dn}{dt} + \nabla_{\parallel} u_{\parallel} + \left(1 + \eta_{\perp} \frac{\hat{v}_{\perp}^2}{2}\right) \frac{1}{L_n} \frac{\partial \Psi}{\partial y} = 0, \quad (1)$$

author's e-mail: kasuya@riam.kyushu-u.ac.jp

$$\frac{du_{//}}{dt} + \nabla_{//}(\tau n + T_{//} + \Psi) = 0, \quad (2)$$

$$\frac{1}{\tau} \frac{dT_{//}}{dt} + \nabla_{//} \left(2u_{//} + \frac{q_{//}}{\tau} \right) + \eta_{//} \frac{1}{L_n} \frac{\partial \Psi}{\partial y} = -\frac{2v_{ii}}{3\tau} (T_{//} - T_{\perp}), \quad (3)$$

$$\frac{1}{\tau} \frac{dT_{\perp}}{dt} + \nabla_{//} \frac{q_{\perp}}{\tau} + \left[\frac{\hat{\nabla}_{\perp}^2}{2} + \eta_{\perp} \left(1 + \hat{\nabla}^2 \right) \right] \frac{1}{L_n} \frac{\partial \Psi}{\partial y} = \frac{v_{ii}}{3\tau} (T_{//} - T_{\perp}), \quad (4)$$

where n is the ion density, $u_{//}$ is the ion velocity, T is the ion temperature, τ is the ratio between ion and electron temperature at the plasma center, η is the ratio between the density and temperature gradient lengths, and the subscripts $//$ and \perp represent the quantities in the parallel and perpendicular directions to the magnetic field, respectively. The other definitions of the parameters are described in Ref. [14]. The gyro-averaged potential Ψ is represented as $\Psi \equiv \Gamma_0^{1/2} \phi$ with operators $\Gamma_0^{1/2} = (1 + b\tau/2)^{-1}$ and $b = -\nabla_{\perp}^2$. Operator b gives the square of the perpendicular wavenumber k_{\perp}^2 , which corresponds to the magnitude of the FLR effect. Two modified Laplacian operators $\hat{\nabla}_{\perp}^2$ and $\hat{\nabla}^2$ are introduced to include the FLR effects. The quasi-neutrality relation is given to be

$$\Gamma_0 \left(n - \frac{b/2}{1 + b\tau/2} T_{\perp} \right) - (1 - \Gamma_0) \frac{\Psi}{\tau} = \Psi \quad (5)$$

to determine the relation between the density and potential.

The Fourier-Bessel expansion is used to calculate 3-D eigenmode structures. The Bessel expansion in the r direction and Fourier expansions in the θ , z directions are applied on Eqs. (1) - (5) by using

$$f(r, \theta, z) = \sum_{m=-M}^M \sum_{j=1}^J \sum_{l=1}^L f_{mjl} J_{mj}(r) e^{im\theta} \times \cos \left(\frac{\pi}{2} (2l-1) \frac{z}{L_z} \right), \quad (6)$$

$$u_{//}(r, \theta, z) = \sum_{m=-M}^M \sum_{j=1}^J \sum_{l=1}^L u_{//mjl} J_{mj}(r) e^{im\theta} \times \sin \left(\frac{\pi}{2} (2l-1) \frac{z}{L_z} \right), \quad (7)$$

where f implies $\{n, T_{//}, T_{\perp}, \phi\}$. Bessel functions

$$J_{mj}(r) \equiv J_m(\lambda_{mj} r/a) \quad (8)$$

are used for the expansion to satisfy the radial boundary conditions $\{\phi, n, u, T_{//}, T_{\perp}\} = 0$ at $r/a = 0, 1$ for perturbation components, where J_m is the m -th Bessel function, λ_{mj} is the j -th point satisfying $J_m(\lambda_{mj}) = 0$, m and l are the azimuthal and axial mode numbers, respectively, a is the plasma radius and L_z is the device length. Fourier expansions are used in the azimuthal and axial directions for simplicity, in spite of existence of the axial boundary determined at the position of the end plate. The set of model

equations is the linearized one, but the radial components with different js are not independent to each other, due to the $(1/r)$ terms, as in $\partial \Psi / \partial y = (1/r) \partial \Psi / \partial \theta$.

For simulations, experimental parameters in PANTA [10] are used; device length $L_z = 4.0$ m, plasma radius $a = 0.07$ m, density $n_0 = 1.0 \times 10^{19} \text{ m}^{-3}$, $L_n = 0.07$ m, $v_{ii} = 350 \text{ s}^{-1}$, magnetic field $B = 0.1$ T, temperatures $T_{e0} = 3 \text{ eV}$ and $T_{i0} = 0.3 \text{ eV}$. The temperatures and magnetic field give $\rho_s = 1.1 \text{ cm}$, $\rho_i = 3.5 \text{ mm}$ and $\Omega_{ci}/2\pi = 3.8 \times 10^4 \text{ Hz}$ for argon plasmas. Here L_n (and η) is set to be constant in space. We concentrate on the mode structure restricted by the plasma radial boundaries, so this simplification is used.

3. Finite-Larmor-Radius Effect

To obtain an analytical form of dependency of ITG instability, the local model with linearization $d/dt \rightarrow -i\omega$, $\nabla_{//} \rightarrow ik_z$, $\partial/\partial y \rightarrow ik_{\theta}$ gives the following dispersion relation from Eqs. (1 - 5);

$$\omega^3 - \omega_1 \omega^2 + P_1 \omega + P_2 = 0, \quad (9)$$

where

$$\omega_1 = \frac{2\tau}{3} \left[-A_2 F + \left(\frac{3}{2\tau} - F \right) (1 + \eta b_1) \right] \frac{\omega_*}{A_1}, \quad (10a)$$

$$P_1 = -\frac{2\tau}{3} k_z^2 \left[\frac{5}{2} + \frac{1}{A_1} \left(\frac{3}{2\tau} - F \right) \right], \quad (10b)$$

$$P_2 = -\frac{2\tau}{3} k_z^2 (1 + F\tau) A_2 \frac{\omega_*}{A_1}, \quad (10c)$$

$$A_1 = \left(b + \frac{b^2\tau}{4} \right) (\tau + 1) + 1, \quad (10d)$$

$$A_2 = -1 + b_1 + \left(\frac{3}{2} - b_1 + b_2 \right) \eta, \quad (10e)$$

$$F = \frac{b/2}{1 + b\tau/2}, \quad (10f)$$

$$b_1 = -\frac{b\tau/2}{1 + b\tau/2}, \quad (10g)$$

$$b_2 = 2b_1 + \frac{b^2\tau^2/2}{(1 + b\tau/2)^2}, \quad (10h)$$

$$\omega_* = \frac{k_{\theta}}{L_n}. \quad (10i)$$

Here $T_{\perp} = T_{//}$ is used for simplicity. In the case with $k_z^2 \ll 1$, Eq. (9) is rewritten to be

$$(\omega - \omega_1 - \delta\omega)(\omega^2 + \delta\omega\omega + T_1) = 0, \quad (11)$$

by use of small $\delta\omega$, where

$$\delta\omega = -\frac{P_1\omega_1 + P_2}{\omega_1^2 + P_1}, \quad (12a)$$

$$T_1 = \frac{P_1^2 - P_2\omega_1}{\omega_1^2 + P_1}. \quad (12b)$$

An unstable ITG mode (slow wave mode) is given in the condition;

$$\delta\omega^2 - 4T_1 \sim -4T_1 < 0, \quad (13)$$

and in the case with $\eta \sim 1$ and small τ ,

$$T_1 \sim -\frac{P_2}{\omega_1} \quad (14)$$

gives the following reduced condition;

$$A_2 > 0. \quad (15)$$

From this inequality, the threshold value η_c is given as

$$\eta_c = \frac{2}{3} + \frac{5}{9}b\tau. \quad (16)$$

This is the threshold value of the unstable ITG mode for the parameters of the linear device in Sec. 2.

The critical value η_c changes depending on the magnitude of τ . This dependency is related to the FLR effect. In the case with $b_2 = 0$ the FLR effect is smaller and the τ dependency of the threshold becomes weaker;

$$\eta_c = \frac{2}{3} + \frac{1}{9}b\tau. \quad (17)$$

Without the FLR effect, $b = 0$, no dependency on τ appears as

$$\eta_c = \frac{2}{3}, \quad (18)$$

which is the well-known threshold of the ITG mode.

In the case of the resistive drift wave instability, which can be unstable in the parameter set of linear devices, break of the Boltzmann relation $n \neq \Psi$ is important for the destabilization [16]. In this model, the FLR effect can break the Boltzmann relation, as Eq. (5), which affects the instability. Equation (5) is transformed to

$$\Psi = \frac{1}{A_1} (n - FT_{\perp}). \quad (19)$$

The 2nd term in the right hand side of Eq. (19) corresponds to the break. Inclusion of higher order $\delta\omega$ terms in Eq. (11) gives the relation for $\delta\omega$ as

$$2\omega_1\delta\omega^2 + (P_1 + \omega_1^2)\delta\omega + P_1\omega_1 + P_2 = 0. \quad (20)$$

If

$$(P_1 + \omega_1^2)^2 - 8\omega_1(P_1\omega_1 + P_2) < 0 \quad (21)$$

is satisfied, a ITG mode (fast wave mode) becomes unstable, but in $\eta = 0$ case, this condition cannot be satisfied, as function F in Eq. (10f) gives $\tau F < 1$. On the other hand, small τ limit gives $F \sim b/2$, and using this form, condition (21) can be satisfied with $\tau \sim 1$, but this is incorrect application of the small τ approximation. The break by the FLR effect is not strong enough, so this effect alone cannot make the mode unstable.

4. Mode Structure

The numerical analysis for the global model using the set of Eqs. (1-5) considers the boundary condition to determine the radial mode structure. Figure 1 shows the

radial eigenmode structures of n , T_{\perp} and ϕ . These radially broad modes with azimuthal mode number $m = 2$ and axial mode number $l = 1$ are most unstable with the plasma parameters in Sec. 2. The values of the perpendicular wavenumber, which is a parameter in local stability analyses, can be evaluated from the radial structure [14]. The mode includes several Bessel components. Figure 2 shows spectra with the radial mode number j . The component with $j = 1$ is dominant, and the dependency on η shows that amplitudes of the components with larger j become smaller with larger η . The dominant mode has $k_{\perp}\rho_i = 0.6 < 1$, so the Padé approximation for the gyro-averaged potential is appropriate. Existence of components with larger j makes the mode structure rather radially steeper in the cases with larger η .

The dependency of the growth rate on τ and η are shown in Fig. 3 (a). The ITG instability is unstable when the ratio of the ion temperature gradient to the density gradient η exceeds the threshold value η_c . The dashed line in Fig. 3 (b) represents the threshold in Eq. (16), which well describes the numerical result. Figure 4 shows comparison of η_c in Figs. 3 (a) and 3 (b). The local analysis, as in Fig. 3 (b), confirms to reproduce the global analysis re-

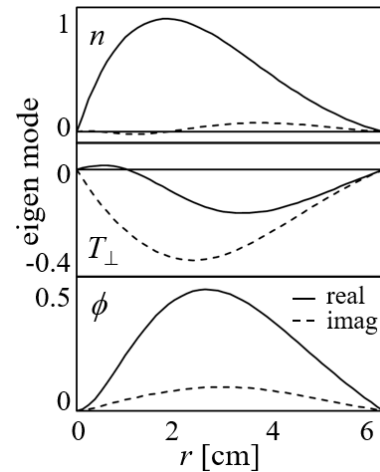


Fig. 1 Radial eigenmode structures with $m = 2$, $l = 1$, $\eta = 1.0$, $\tau = 0.5$. Radial profiles of n , T_{\perp} and ϕ are shown, where solid and dashed lines represent the real and imaginary parts, respectively.

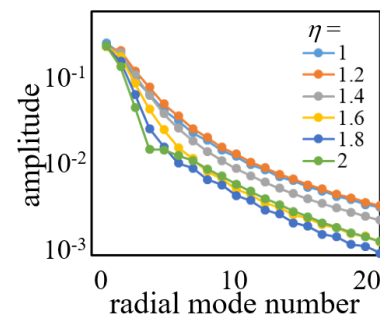


Fig. 2 Dependency of the radial mode number spectra on η with $m = 2$, $l = 1$, $\tau = 0.5$.

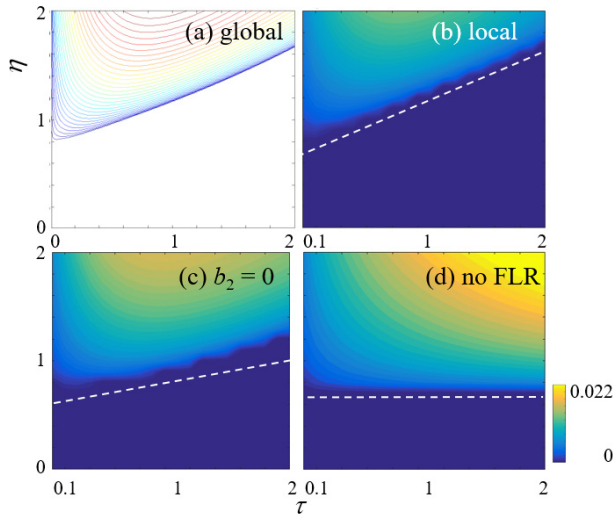


Fig. 3 Dependency of the growth rate on τ and η with $m = 2$, $l = 1$. The results of the (a) global analysis, (b) local, (c) local with $b_2 = 0$ and (d) local without the FLR effect are plotted. The dashed lines represent the analytical expressions of the thresholds.

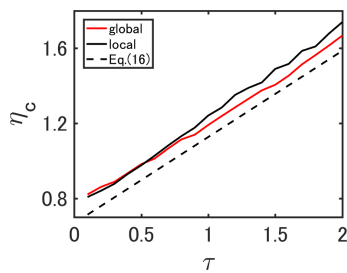


Fig. 4 Comparison of the thresholds for the ITG instability from the global and local models with $m = 2$, $l = 1$. The dashed line represents the analytical expression in Eq. (16).

sult by adjusting the wavenumber to that obtained from the global analysis.

The dependency of η_c on τ is confirmed numerically in the smaller or no FLR effect cases with $b_2 = 0$ (Fig. 3 (c)) and (Fig. 3 (d)), whose analytical forms with the local model are given in Eqs. (17) and (18), respectively.

5. Summary

Numerical analyses using a gyro-fluid model have been performed to investigate the FLR effect on ITG instability in cylindrical plasmas. A spectrum code with Fourier-Bessel expansion has been developed for the analysis of global mode structures. The analytical expression of η_c is obtained from the local dispersion relation. Its τ dependency comes from the FLR effect. The ratio between ion and electron temperatures is an important parameter for plasma performance in torus devices [17], and the ITG instability threshold is investigated using fluid and kinetic approaches [18]. In torus configurations, resonance with magnetic drift appears to give a toroidal ITG mode

with stronger threshold dependence on τ [19]. In linear devices the magnetic field is homogeneous, so the target in this article is a slab ITG mode, which is induced by compressibility with parallel ion motion. The FLR terms include τ dependency related to orbit averaging on Ψ , which gives the threshold dependency. Break of the Boltzmann relation by the FLR effect is not strong as to generate another unstable branch of the ITG mode, so resistivity is rather important with the parameter set of linear devices to break the Boltzmann relation, which excites the resistive drift wave [11].

Linear characteristics have been confirmed with constant background density and temperature gradients. We are developing the code to include the background profiles, in which couplings between different Bessel components must be considered. The routine can be extended to apply to nonlinear calculation, which will be carried out for investigating dynamics in turbulent plasmas. Torus devices are used for fusion researches, and for investigation of global structures and their dynamics in torus, PLATO project is now progressing to establish a plasma turbulence observatory [20]. Construction of the platform for analyzing 3-D dynamics of plasma instabilities with a variety of simulation codes is necessary for comparison between experiments and simulations both in cylindrical and torus plasmas.

Acknowledgments

This work was partly supported by JSPS KAKENHI Grant Number (JP16K06938, JP17H06089), by the collaboration program of NIFS (NIFS19KNST144, NIFS18KNXN373) and RIAM of Kyushu University.

- [1] X. Garbet *et al.*, Nucl. Fusion **50**, 043002 (2010).
- [2] R.E. Waltz *et al.*, Phys. Plasmas **4**, 2482 (1997).
- [3] J.E. Kinsey *et al.*, Phys. Plasmas **12**, 052503 (2005).
- [4] G.M. Staebler *et al.*, Phys. Plasmas **14**, 055909 (2007).
- [5] R.E. Waltz *et al.*, Phys. Plasmas **1**, 2229 (1994).
- [6] A. Kendl *et al.*, Phys. Plasmas **17**, 072302 (2010).
- [7] P.H. Diamond *et al.*, Plasma Phys. Control. Fusion **47**, R35 (2005).
- [8] G.R. Tynan *et al.*, Plasma Phys. Control. Fusion **51**, 113001 (2009).
- [9] A.K. Sen *et al.*, Phys. Rev. Lett. **66**, 429 (1991).
- [10] S. Inagaki *et al.*, Sci. Repts. **6**, 22189 (2016).
- [11] N. Kasuya, M. Yagi, K. Itoh and S.-I. Itoh, Phys. Plasmas **15**, 052302 (2008).
- [12] Y. Miwa *et al.*, Plasma Fusion Res. **8**, 2403133 (2013).
- [13] G. Hattori *et al.*, Plasma Fusion Res. **10**, 3401060 (2015).
- [14] T. Ohno *et al.*, Plasma Fusion Res. **13**, 1401081 (2018).
- [15] W. Dorland and W. Hammet, Phys. Fluids B **5**, 812 (1993).
- [16] A. Hasegawa and M. Wakatani, Phys. Rev. Lett. **50**, 682 (1983).
- [17] C.C. Petty *et al.*, Phys. Rev. Lett. **83**, 3661 (1999).
- [18] J. Weiland, *Collective Modes in Inhomogeneous Plasma* (Institute of Physics, Bristol, 2000).
- [19] A. Casati *et al.*, Phys. Plasmas **15**, 042310 (2008).
- [20] A. Fujisawa, AIP Conf. Proc. **1993**, 020011 (2018).